Resonant hyper-Raman scattering in spherical quantum dots

E. Menéndez-Proupin and C. Trallero-Giner
Departamento de Física Teórica, Universidad de La Habana, Vedado 10400, La Habana, Cuba

A. García-Cristobal
Departamento de Física Aplicada, Universidad de Valencia, E-46100 Burjassot, Spain
(Received 27 July 1998; revised manuscript received 8 December 1998)

A theoretical model of resonant hyper-Raman scattering by an ensemble of spherical semiconductor quantum dots has been developed. The electronic intermediate states are described as Wannier-Mott excitons in the framework of the envelope function approximation. The optical polar vibrational modes of the nanocrystallites (vibrons) and their interaction with the electronic system are analyzed with the help of a continuum model satisfying both the mechanical and electrostatic matching conditions at the interface. An explicit expression for the hyper-Raman scattering efficiency is derived, which is valid for incident two-photon energy close to the exciton resonances. The dipole selection rules for optical transitions and Fröhlich-like exciton-lattice interaction are derived: It is shown that only exciton states with total angular momentum $L=0,1$ and vibrational modes with angular momentum $l_p=1$ contribute to the hyper-Raman scattering process. The scattering spectrum and resonance profile are calculated for spherical CdSe zinc-blende-type nanocrystals. Their dependence on the dot radius and the influence of the size distribution on them are also discussed.
[S0163-1829(99)00628-1]

I. INTRODUCTION

The research on semiconductor quantum dots (QD's) has undergone a dramatic increase in recent years, stimulated by their foreseen applications in optics and electronics technology and also due to their nonlinear optical properties.[1] Quantum dot systems based on III-V materials as well as nanocrystallites of II-VI compounds embedded in glass have been thoroughly investigated (for a review see Ref. 2). Among the scattering mechanisms present in polar semiconductors, the optical phonon emission is known to play a dominant role in QD's, which can be experimentally investigated by employing a number of methods, such as infrared absorption and Raman scattering.[3–10] The successful interpretation of light scattering by optical phonons relies upon a good knowledge of the normal vibrational modes. In recent years a phenomenological continuum theory of optical phonons in nanostructures has been elaborated,[11–13] which is in good agreement with *ab initio* calculations and allows us to explain the resonant Raman-scattering intensities of phonon modes induced by interface roughness in quantum wells.[14] The theory has also been generalized to deal with quantum wires and quantum dots, and used to study resonant Raman scattering in these systems.[15–17] In particular, the formalism is applicable to II-VI semiconductor nanocrystallites embedded in glass since they can have dimensions as small as 13 Å, in which case the mechanical confinement of optical vibrational modes has strong effects (in a QD the concept of phonon as an excitation in a periodic system labeled by a wave vector is lost, and, therefore, we will use the term *vibron* to denote the QD vibrational modes). Raman scattering provides a useful tool to investigate experimentally these vibrons, but only spherically symmetric modes are accessible to this technique. In the search of complementary experimental techniques, which can overcome this limitation, hyper-Raman (HR) spectroscopy appears to be a suitable candidate.[18] Recently, HR spectroscopy has been used to study the optical vibrational modes of CdS and CuBr QD's.[19–21] In this paper we present a theoretical model that allows us to study hyper-Raman scattering (HRS) by optical vibrons under resonance conditions, and illustrate it by performing numerical calculations of the scattered intensities in CdSe nanocrystallites. As far as the exciton-lattice interaction is concerned only the Fröhlich coupling is considered here, though it is admitted that the deformation potential interaction might be of importance for photon energies far from the excitonic resonances. The selection rules for the scattering process are worked out and it is shown that in fact HRS can be used to probe optical vibrations with nonspherical symmetry.

The paper is organized as follows: The main concepts underlying the hyper-Raman scattering and the description of the nanocrystal vibrational modes and excitons are outlined in Sec. II. Section III contains the theoretical expressions for the matrix elements and HRS efficiency, which are used to analyze the selection rules of the scattering process. In Sec. IV the calculation of the exciton and vibrational spectra of CdSe nanocrystallites are presented, and the numerical results obtained for the HRS efficiency are also discussed. Section V is devoted to the main conclusions of the work and final comments.

II. THEORY

Hyper-Raman scattering is a nonlinear process that consists of the absorption of two photons of frequency ω_i, wave vector $\vec{k}_i$, and polarization $\vec{e}_i$ $(i=1,2)$, and the emission of one photon $(\omega_s,\vec{k}_s,\vec{e}_s)$ with the simultaneous excitation of a number of vibrational modes.[22] Due to its nonlinear nature, it is convenient to express the HR yield by the normalized (intensity-independent) scattering cross section,[23]

$$\frac{1}{I_i}\frac{d^2\sigma^{ij}}{d\omega_s d\Omega_s}=\frac{1}{I_i I_j}\frac{d^2P_{ij}}{d\omega_s d\Omega_s}, \tag{1}$$

I_i and I_j being the excitation intensities and $d^2P_{ij}/d\omega_s d\Omega_s$ being the scattered power per unit of solid angle Ω_s and unit frequency. The scattered power can be related to the probability per unit time of a single scattering event in a QD of radius R, so that we can express the normalized differential cross section as[23]

$$\frac{1}{I_i}\frac{d^2\sigma^{ij}}{d\omega_s d\Omega_s}=\frac{V^3}{(2\pi)^2}\frac{\omega_s^3\eta_i\eta_j\eta_s^3}{\hbar^3\omega_j\omega_i c^5}\times\sum_p |M_p(\omega_i,\omega_j,\omega_s;R)|^2\times\delta(\omega_i+\omega_j-\omega_p-\omega_s), \tag{2}$$

where V is the normalization volume, η_i $(i=1,2)$ and η_s are the nanocrystal refraction indices at ω_i and ω_s, respectively, c is the velocity of light in vacuum, and M_p is the scattering amplitude. Each scattering event is accompanied by the emission of a vibron of frequency ω_p, and the total scattering probability is obtained after summing over all possible vibron states p. Only vibron emission (Stokes) processes will be considered in this paper. The delta function in Eq. (2) can be eventually replaced by a Lorentzian $\Delta(\omega_s)$ with a vibron lifetime $\tau_p=\hbar/\Gamma_p$ on the line broadening of the HR spectrum.

The scattering amplitude in Eq. (2) can be calculated in fourth-order perturbation theory. Under resonance conditions the important contributions to M_p are given by

$$M_p^{(a)}=\sum_{\mu_1,\mu_2,\mu_3}\frac{\langle F|\hat{H}_{E-R}^{(s)}|\mu_3\rangle\langle\mu_3|\hat{H}_{E-L}|\mu_2\rangle\langle\mu_2|\hat{H}_{E-R}^{(j)}|\mu_1\rangle\langle\mu_1|\hat{H}_{E-R}^{(i)}|I\rangle}{(\hbar\omega_s-E_{\mu_3}+i\Gamma_{\mu_3})(\hbar\omega_i+\hbar\omega_j-E_{\mu_2}+i\Gamma_{\mu_2})(\hbar\omega_i-E_{\mu_1}+i\Gamma_{\mu_1})}. \tag{3}$$

The exciton created in the state $|\mu_1\rangle$ after the absorption of a photon $(\omega_i,\vec{k}_i,\vec{e}_i)$ is first scattered to the state $|\mu_2\rangle$ by the absorption of a second photon $(\omega_j,\vec{k}_j,\vec{e}_j)$. In the next step, the interaction with the lattice induces an excitonic transition from $|\mu_2\rangle$ to $|\mu_3\rangle$, accompanied by the creation of a vibron of frequency ω_p. The exciton finally recombines emitting a photon $(\omega_s,\vec{k}_s,\vec{e}_s)$. In Eq. (3), $|I\rangle$ ($|F\rangle$) is the initial (final) state of the scattering process, and E_{μ_i} and Γ_{μ_i} are the energies and lifetime broadenings of the excited electronic states $|\mu_i\rangle$ in the QD. $\hat{H}_{E-L}$ and $\hat{H}_{E-R}$ are the Hamiltonian operators for the interaction of the electronic system with the lattice and radiation field, respectively.

Since the interesting range of $\hbar\omega_i+\hbar\omega_j$ for resonant HR spectroscopy lies around the fundamental absorption edge of the QD E_g+E_0, the relevant resonances in the matrix element (3) will occur at energies $\hbar\omega_i+\hbar\omega_j=E_{\mu_2}$ and $\hbar\omega_s=E_{\mu_3}$ (outgoing resonance).

Another contribution to the scattering amplitude is

$$M_p^{(b)}=\sum_{\mu_1,\mu_2,\mu_3}\frac{\langle F|\hat{H}_{E-R}^{(s)}|\mu_3\rangle\langle\mu_3|\hat{H}_{E-R}^{(j)}|\mu_2\rangle\langle\mu_2|\hat{H}_{E-L}|\mu_1\rangle\langle\mu_1|\hat{H}_{E-R}^{(i)}|I\rangle}{(\hbar\omega_s-E_{\mu_3}+i\Gamma_{\mu_3})(\hbar\omega_i-\hbar\omega_p-E_{\mu_2}+i\Gamma_{\mu_2})(\hbar\omega_i-E_{\mu_1}+i\Gamma_{\mu_1})}. \tag{4}$$

The examination of the energy denominators in Eq. (4) clearly indicates that $|M_p^{(b)}|\ll|M_p^{(a)}|$ in the resonance region $\hbar\omega_i+\hbar\omega_j\sim E_g+E_0$. Therefore, the contribution from $M_p^{(b)}$ has been dropped out from our theoretical model.

Finally, it must be noted that in real samples the nanocrystallites present a distribution over size and shape. We intend to study here HRS by an ensemble of spherical QD's characterized by a distribution over radii $F(R)$. The corresponding average (intensity-independent) HRS efficiency[3] is given by

$$\left\langle\frac{d^2S_{HR}^{ij}}{d\omega_s d\Omega_s}\right\rangle=\frac{1}{\langle V_D\rangle}\int\frac{1}{I_i}\frac{d^2\sigma^{ij}}{d\omega_s d\Omega_s}F(R)dR, \tag{5}$$

where $\langle V_D\rangle$ is the average quantum dot volume.

The intermediate electronic virtual states appearing in the HR process [see Eq. (3)] are taken to be size-confined Wannier-Mott excitons, treated in the framework of the envelope function approximation. The details of this approach can be found in Ref. 17, where it is employed for the study of resonant Raman scattering in QD's. We summarize here, for notation purposes, the main expressions of the exciton model.

The eigenfunctions of the full Hamiltonian including the electron-hole Coulomb interaction (exciton wave functions) are expanded in terms of the electron-hole pair (EHP) states $\Phi_{\alpha,L,M}(\vec{r}_e,\vec{r}_h)$,[17]

$$\Psi_\mu(\vec{r}_e,\vec{r}_h)\equiv\Psi_{N,L,M,P}(\vec{r}_e,\vec{r}_h)=\sum_\alpha C_{N,L,M,P}(\alpha)\Phi_{\alpha,L,M}(\vec{r}_e,\vec{r}_h), \tag{6}$$

where N,L,M, and P are the quantum numbers corresponding to the energy, the squared total angular momentum $\hat{L}^2$, its projection along the z axis $\hat{L}_z$, and the inversion operator, respectively. α is an abbreviated notation for $\alpha\equiv(n_e,n_h,l_e,l_h)$. Note that the state defined by Eq. (14) has definite parity: $P=1$ (even parity) if l_e+l_h is even and $P=-1$ (odd parity) if l_e+l_h is odd.

In polar materials, the long-range electrostatic field associated with the optical vibrations introduces the Fröhlich mechanism. It is now well established that despite its dipole-forbidden character,[3] the Fröhlich interaction plays an important role in one-phonon Raman scattering by bulk zincblende semiconductors.[24] On the other hand, in systems which *lack translational invariance*, like QD's, Fröhlich-induced Raman scattering becomes allowed and, therefore, it plays a dominant role. Accordingly, in our model for the HRS we consider only the Fröhlich-like interaction between excitons and vibrons. In order to describe the polar optical vibrational modes (vibrons) of spherical QD's we rely upon the results of Ref. 15, where a macroscopic continuum model coupling the mechanical displacement and the electrostatic potential is developed. The normal modes are labeled by a set of integer numbers $p\equiv(n_p,l_p,m_p)$, which are related to their symmetry properties. More details on the calculation of the displacement, electrostatic potential and frequency ω_{n_p,l_p} associated to these modes can be found in Refs. 15 and 16. The exciton-vibron interaction Hamiltonian operator can be written as

$$\hat{H}_{E-L}=e\hat{\varphi}_F(\vec{r}_e)-e\hat{\varphi}_F(\vec{r}_h), \tag{7}$$

where $-e$ $(e>0)$ is the electron charge and

$$e\hat{\varphi}_F(\vec{r})=\frac{C_F}{\sqrt{R}}\sum_{n_p,l_p,m_p}\sqrt{\frac{\omega_L}{\omega_{n_p,l_p}}}\Phi_{n_p,l_p}(r) \times[Y_{l_p,m_p}(\Omega)\hat{b}_{n_p,l_p,m_p}+\text{H.c.}]. \tag{8}$$

Here, $\hat{b}_{n_p,l_p,m_p}$ is the vibron annihilation operator, C_F is the Fröhlich constant, and H.c. means Hermitian conjugate. The explicit form of the radial function $\Phi_{n_p,l_p}(r)$ can be found in Ref. 16, and $Y_{l_p,m_p}(\Omega)$ ($l=0,1,\ldots,$ and $m=-l,\ldots,l$) are the spherical harmonics.[25] Since $\omega_{n_p,l_p}\sim\omega_L$ (ω_L is the bulk LO phonon frequency at the Γ point), we will omit hereafter the factor $\sqrt{\omega_L/\omega_{n_p,l_p}}$ in Eq. (8).

III. MATRIX ELEMENTS AND SELECTION RULES

In this section we analyze in detail the matrix elements appearing in Eq. (3), and derive from them the selection rules for the exciton and vibron states which participate in the HR process. The matrix elements $\langle\mu_1|\hat{H}^{(i)}_{E-R}|I\rangle$ and $\langle F|\hat{H}^{(s)}_{E-R}|\mu_3\rangle$ for direct allowed optical transitions between valence (v) and conduction (c) bands are proportional to the exciton overlap integral given by[17]

$$f_\mu\equiv f_{N,L,M,P}=\int\Psi_{N,L,M,P}(\vec{r},\vec{r})d^3\vec{r} =\delta_{L,0}\delta_{M,0}\delta_{P,1}\sum_{n_e,n_h}\sum_l(-1)^l\sqrt{2l+1} \times C_{N,0,0,1}(n_e,n_h,l,l)\int_0^\infty R_{n_e,l}(r)R_{n_h,l}(r)r^2dr, \tag{9}$$

where $R_{n,l}(r)$ is the radial part of the single-particle wave function. Hence, the annihilation of the first incoming photon with frequency ω_i creates an exciton in the state with zero angular momentum and even parity $\mu_1\equiv(N_1,L_1=0,M_1=0,P_1=1)$, and analogously, the scattered photon of frequency ω_s is emitted upon the recombination of an exciton in the state $\mu_3\equiv(N_3,L_3=0,M_3=0,P_3=1)$. Both exciton states have $L=0$ and $P=1$ because the interband transitions induced by the radiation field require the electron and hole to have equal orbital angular momentum quantum numbers $l_e=l_h$.

A different situation is found when considering the scattering between exciton states induced by the second incoming photon [matrix element $\langle\mu_2|\hat{H}^{(j)}_{E-R}|\mu_1\rangle$ in Eq. (3)]. We can consider only *intraband excitonic transitions*, whose matrix element can be written, in the dipole approximation,[26] as

$$\langle\mu_2|\hat{H}^{(j)}_{E-R}|\mu_1\rangle=\int\Psi^*_{\mu_2}(\vec{r}_e,\vec{r}_h)(\hat{H}^{(j)}_{e-R}-\hat{H}^{(j)}_{h-R}) \times\Psi_{\mu_1}(\vec{r}_e,\vec{r}_h)d^3\vec{r}_e d^3\vec{r}_h, \tag{10}$$

where

$$\hat{H}^{(j)}_{\nu-R}=\frac{e}{m_\nu}\frac{1}{\sqrt{V}}\sqrt{\frac{2\pi\hbar}{\omega_j\eta_j^2}}(\vec{e}_j\cdot\hat{\vec{p}}_\nu)\quad(\nu=e,h), \tag{11}$$

$\hat{\vec{p}}_\nu=-i\hbar\vec{\nabla}_\nu$ is the linear momentum operator, and m_e (m_h) is the electron (hole) effective mass (taken to be positive).

Using expansion (6) in Eq. (10) we get

$$\langle\mu_2|\hat{H}^{(j)}_{E-R}|\mu_1\rangle =e\frac{1}{\sqrt{V}}\sqrt{\frac{2\pi\hbar}{\omega_j\eta_j^2}}\sum_{\alpha,\alpha'}C^*_{N_2,L_2,M_2,P_2}(\alpha')C_{N_1,L_1,M_1,P_1}(\alpha) \times\left\langle\alpha',L_2,M_2\left|\frac{\vec{e}_j\cdot\hat{\vec{p}}_e}{m_e}-\frac{\vec{e}_j\cdot\hat{\vec{p}}_h}{m_h}\right|\alpha,L_1,M_1\right\rangle. \tag{12}$$

Let us now concentrate on the electron part of the matrix element appearing in Eq. (12). By making use of the operator identity $\hat{\vec{p}}_e=(im_e/\hbar)[\hat{H}_e,\vec{r}_e]$, where $\hat{H}_e$ is the single-electron Hamiltonian, we have found that (see Appendix)

$$\left\langle n'_e,n'_h,l'_e,l'_h,L_2,M_2\left|\frac{\vec{e}\cdot\hat{\vec{p}}_e}{m_e}\right|n_e,n_h,l_e,l_e,0,0\right\rangle =\delta_{n'_h,n_h}\delta_{l'_h,l_h}\delta_{L_2,1}\delta_{P_2,-1}a_{M_2}\frac{iR}{\hbar}\frac{1}{\sqrt{3}}(E_{n'_e,l'_e}-E_{n_e,l_e}) \times\left[\sqrt{\frac{l_e+1}{2l_e+1}}\delta_{l'_e,l_e+1}-\sqrt{\frac{l_e}{2l_e+1}}\delta_{l'_e,l_e-1}\right] \times G_{n_e,l_e\to n'_e,l'_e}, \tag{13}$$

$$G_{n,l\to n',l'}=\frac{1}{R}\int_0^\infty R_{n',l'}(r)R_{n,l}(r)r^3dr. \tag{14}$$

The final expression for the matrix element (12) can be arranged in the form

$$\langle \mu_2|\hat{H}^{(j)}_{E-R}|\mu_1\rangle = \frac{ieE_0\overline{R}^2}{\hbar R}\frac{1}{\sqrt{V}}\sqrt{\frac{2\pi\hbar}{\omega_j\eta_j^2}}[\mathcal{F}^{(e)}_{\mu_1\to\mu_2}-\mathcal{F}^{(h)}_{\mu_1\to\mu_2}], \tag{15}$$

where we have introduced the energy $E_0=\hbar^2/2m_0\overline{R}^2$ ($\overline{R}$ is the average QD radius) to make $\mathcal{F}^{(e,h)}$ dimensionless. The explicit expression for $\mathcal{F}^{(e)}_{\mu_1\to\mu_2}$ is

$$\begin{aligned}\mathcal{F}^{(e)}_{\mu_1\to\mu_2} &= \delta_{L_2,1}\delta_{P_2,-1}a_{M_2}\\ &\times\sum_{\alpha,\alpha'}\delta_{l_e,l_h}\delta_{l'_h,l_h}\delta_{n'_h,n_h}C^*_{\mu_2}(\alpha')C_{\mu_1}(\alpha)\\ &\times\left(\frac{R}{\overline{R}}\right)^2\frac{(E_{n'_e,l'_e}-E_{n_e,l_e})}{\sqrt{3}E_0}\left[\sqrt{\frac{l_e+1}{2l_e+1}}\delta_{l'_e,l_e+1}\right.\\ &\left.-\sqrt{\frac{l_e}{2l_e+1}}\delta_{l'_e,l_e-1}\right]G_{n_e,l_e\to n'_e,l'_e}.\end{aligned} \tag{16}$$

A similar expression holds for $\mathcal{F}^{(h)}_{\mu_1\to\mu_2}$ after the exchange of the subscripts e and h.

An important consequence to be drawn from Eq. (16) is that after the absorption of the second incoming photon, the exciton must be in the state $\mu_2\equiv(N_2,L_2=1,M_2=0,\pm1,P_2=-1)$. Otherwise stated, two-photon absorption generates excitons in $L=1$ states, in contrast to one-photon transitions for which the final exciton state is necessarily $L=0$. Moreover, the factor $\delta_{l',l\pm1}$ in Eq. (16) introduces the parity selection rule $P_1=1\to P_2=-1$, indicating that the intraband transitions are accompanied by a change in the parity of the excitonic state. If the incident light is linearly polarized with $\vec{e}_j\|\hat{z}$ then $a_{M_2}=\delta_{M_2,0}$ (see the Appendix), whereas for circular polarization $\vec{e}_j\|(\hat{x}\pm i\hat{y})/\sqrt{2}$, we have $a_{M_2}=\delta_{M_2,\pm1}$ ($\hat{x},\hat{y}$, and $\hat{z}$ represent some system of orthogonal axes attached to the laboratory frame). Hence, the $L_2=1$ excitonic states participating in the HRS process have $M_2=0$ for linearly polarized light and $M_2=\pm1$ for circularly polarized light.

Now we turn to the matrix element of the exciton-lattice interaction $\langle\mu_3|\hat{H}_{E-L}|\mu_2\rangle$. If we select the vibron creation terms in Eq. (8) and make use of Eq. (6), we get the expression

$$\begin{aligned}&\langle\mu_3|\hat{H}_{E-L}|\mu_2\rangle\\ &=\frac{C_F}{\sqrt{R}}\sum_{\alpha',\alpha''}C^*_{N_3,L_3,M_3,P_3}(\alpha'')C_{N_2,L_2,M_2,P_2}(\alpha')\\ &\times\sum_{n_p,l_p,m_p}\langle\alpha'',L_3,M_3|\Phi_{n_p,l_p}(r_e)\\ &\times Y^*_{l_p,m_p}(\Omega_e)-\Phi_{n_p,l_p}(r_h)Y^*_{l_p,m_p}(\Omega_h)|\alpha',L_2,M_2\rangle,\end{aligned} \tag{17}$$

which consists again of separated electron and hole contributions, each of them being a sum of matrix elements of spherical tensors. Therefore, the method used previously for the intraband exciton-photon matrix elements applies also here. By following that procedure, and considering that $L_2=1$ and $L_3=M_3=0$, Eq. (17) is reduced to

$$\langle\mu_3|\hat{H}_{E-L}|\mu_2\rangle=\frac{C_F}{\sqrt{R}}[\mathcal{H}^{(e)}_{\mu_2\to\mu_3}-\mathcal{H}^{(h)}_{\mu_2\to\mu_3}], \tag{18}$$

where

$$\begin{aligned}\mathcal{H}^{(e)}_{\mu_2\to\mu_3} &= \delta_{l_p,1}\delta_{m_p,M_2}\\ &\times\sum_{\alpha',\alpha''}\delta_{l''_e,l''_h}\delta_{n''_h,n'_h}\delta_{l''_h,l'_h}C^*_{\mu_3}(\alpha'')C_{\mu_2}(\alpha')\\ &\times\frac{1}{\sqrt{4\pi}}\left[\sqrt{\frac{l''_e+1}{2l''_e+1}}\delta_{l'_e,l''_e+1}\right.\\ &\left.-\sqrt{\frac{l''_e}{2l''_e+1}}\delta_{l'_e,l''_e-1}\right]\Phi^{n_p,l_p}_{n'_e,l'_e\to n''_e,l''_e},\end{aligned} \tag{19}$$

$$\Phi^{n_p,l_p}_{n',l'\to n'',l''}=\int_0^\infty R_{n'',l''}(r)R_{n',l'}(r)\Phi_{n_p,l_p}(r)r^2dr. \tag{20}$$

An expression analogous to Eq. (19) holds for $\mathcal{H}^{(h)}_{\mu_2\to\mu_3}$ after the exchange of the subscripts e and h. It follows from Eq. (19) that the quantum numbers of the emitted vibron are fixed to be $l_p=1$ and $m_p=M_2$. The different states m_p can be discriminated by selecting adequately the polarization $\vec{e}_j$ of the exciting light: $M_2=m_p=0$ if $\vec{e}_j\|\hat{z}$ and $M_2=m_p=\pm1$ if $\vec{e}_j\|(\hat{x}\pm i\hat{y})/\sqrt{2}$. Thus, the HR selection rules in a spherical QD can be expressed schematically by the following sequence of states:

$$\begin{aligned}&(L_1=0,M_1=0)\to(L_2=1,M_2=0,\pm1)\\ &\qquad\xrightarrow{(l_p=1,m_p=M_2)}\quad(L_3=0,M_3=0),\end{aligned} \tag{21}$$

which contrasts with that corresponding to Raman scattering[16,17]

$$(L_1=0,M_1=0)\xrightarrow{(l_p=0,m_p=0)}(L_2=0,M_2=0), \tag{22}$$

where only $l_p=0$ vibrons can be excited. The comparison between Eqs. (21) and (22) makes it clear the complementariness of both light-scattering techniques to study the vibrational spectra of spherical QD's. In particular, we have shown that hyper-Raman spectroscopy can be used to investigate the $l_p=1$ vibronic states, not observable in Raman scattering. In addition, the analysis of the corresponding resonance profiles (scattering efficiency vs $\hbar\omega_i+\hbar\omega_j$) can be useful to reveal $L=1$ exciton states. Of course, the selection rules discussed can be relaxed when going beyond our simplified treatment of the HR process, e.g., including valence band mixing. Nevertheless, for R smaller than the bulk exciton Bohr radius the separation in energy between the *hh* and *lh* levels induced by the confinement should lead to a small amount of *hh*-*lh* admixture.

Finally, by inserting Eqs. (9), (15), and (18) into Eq. (3), we obtain the following compact expression for the normalized scattering cross section:

$$\frac{1}{I_i}\frac{d^2\sigma^{ij}}{d\omega_s d\Omega_s}=\sigma_0\left(\frac{\overline{R}}{R}\right)^3\sum_{n_p}\frac{\eta_s}{\eta_i\eta_j}\frac{\omega_s^2}{\omega_i\omega_j}\times|\mathcal{M}_{n_p}(\omega_i,\omega_j,\omega_s;R)|^2\Delta(\omega_s), \quad (23)$$

where $\mathcal{M}_{n_p}$ is the dimensionless amplitude given by

$$\mathcal{M}_{n_p}=E_0^3\sum_{\mu_1,\mu_2,\mu_3}\frac{f^*_{\mu_3}[\mathcal{H}^{(e)}_{\mu_2\to\mu_3}-\mathcal{H}^{(h)}_{\mu_2\to\mu_3}]}{(\hbar\omega_s-E_{\mu_3}+i\Gamma_{\mu_3})}\times\frac{[\mathcal{F}^{(e)}_{\mu_1\to\mu_2}-\mathcal{F}^{(h)}_{\mu_1\to\mu_2}]f_{\mu_1}}{(\hbar\omega_i+\hbar\omega_j-E_{\mu_2}+i\Gamma_{\mu_2})(\hbar\omega_i-E_{\mu_1}+i\Gamma_{\mu_1})}, \quad (24)$$

$$\sigma_0=2\pi\frac{e^6}{m_0^2c^5}\frac{\overline{R}^2}{\hbar^2\omega_i\omega_j}\frac{|\vec{e}_i\cdot\vec{p}_{cv}|^2|\vec{e}_s\cdot\vec{p}_{cv}|^2}{m_0^2E_0^2}\frac{C_F^2}{E_0^2\overline{R}}. \quad (25)$$

m_0 is the free electron mass, and $\vec{p}_{cv}$ is the interband momentum matrix element between valence and conduction Bloch functions at $\vec{k}=0$. Expression (23) is suitable for the calculation of the scattered spectrum as a function of the HR shift $\omega_s-\omega_i-\omega_j$. If we are interested in the resonance behavior of the scattered intensity we can obtain the average HRS efficiency by integrating Eq. (5) over ω_s,

$$\left\langle\frac{dS^{ij}_{HR}}{d\Omega_s}\right\rangle=\frac{\langle\sigma_0\rangle}{\langle V_D\rangle}\sum_{n_p}\int F(R)\times\frac{[\omega_i+\omega_j-\omega_{n_p}(R)]^2}{\omega_i\omega_j}\frac{\eta_s}{\eta_i\eta_j}\left(\frac{\overline{R}}{R}\right)^3\times|\mathcal{M}_{n_p}(\omega_i,\omega_j,\omega_i+\omega_j-\omega_{n_p}(R);R)|^2dR, \quad (26)$$

where $\langle\sigma_0\rangle$ is the average of σ_0 over the QD orientations in the ensemble with the angle $\arccos(\vec{e}_i\cdot\vec{e}_s)$ fixed.[8] For typical values of $\overline{R}$ ($\sim$20 Å) and E_0 ($\sim$10 meV), and the parameters of Table I a value of 10^{-4} cm MW^{-1} sr^{-1} is estimated for $\langle\sigma_0\rangle/\langle V_D\rangle$.

The total HRS efficiency is obtained making up the sum over topologically nonequivalent diagrams ($i\leftrightarrow j$). From now on we focus on the degenerate case, $i=j$, $\omega_i=\omega_j=\omega_l$, with $2\omega_l$ in the region around the excitonic transitions, which is the usual situation for resonant HRS experiments.

IV. SCATTERING INTENSITIES

In the following we consider the radial part of the single-particle wave functions as the solutions of the infinite barrier spherical well problem. First, we present in Fig. 1(a) the exciton energies in a CdSe QD as a function of the radius. The material parameters used as input are shown in Table I. Solid and dashed lines correspond to $L=0$ and $L=1$ excitons, respectively. According to Ref. 10 we have taken into account the penetration of the wave function in the glass matrix by using an effective radius $R_{ef}=3.367+0.9078R$ (in Å), where R is the nominal QD radius.

TABLE I. Values of the material parameters used for the numerical calculations. The same value Γ_μ (Γ_{n_p}) has been assigned to all exciton (vibron) states.

Parameter	Value
m_e/m_0	0.12[a]
m_h/m_0	0.45[a]
E_g (eV)	1.865[b]
ω_L (cm^{-1})	213.1[b]
ω_T (cm^{-1})	165.2[c]
β_L (10^3 ms^{-1})	2.969[b]
β_T (10^3 ms^{-1})	0.002
ϵ_{a0} (CdSe)	9.53[d]
$\epsilon_{a\infty}$ (CdSe)	5.72[e]
$\epsilon_{b\infty}$ (Glass)	4.64[f]
Γ_μ (meV)	5
Γ_{n_p} (cm^{-1})	2
P^2 (eV)	20[g]

[a]Reference 30.
[b]Reference 10.
[c]Reference 27.
[d]Reference 31.
[e]Calculated from the Lydanne-Sachs-Teller relation.
[f]Reference 32.
[g]Reference 33. $P^2=2|\vec{p}_{cv}|^2/m_0$.

Let us now focus our attention on the vibrational modes. Since the active TO phonon branch of hexagonal CdSe seems to be flat,[27] the parameter β_T appearing in the isotropic model for the optical vibrations has been taken as the limit $\beta_T^2\to 0^+$, with a negative bulk dispersion relation $\omega^2=\omega_T^2-\beta_T^2q^2$. Figure 1(b) illustrates the allowed frequencies for the $l_p=1$ optical vibrons as a function of the QD radius. Below $\omega_L=213$ cm^{-1} the confined LO modes can be seen with both longitudinal and transverse components, including a surface mode contribution.[28] We can observe some bending in the dispersion around 185 cm^{-1}, which is identified as the Fröhlich mode.[29] The Fröhlich frequency ω_F is related only to the dielectric constants of the constituent media: $\omega_F^2=\omega_T^2(\epsilon_{a0}+2\epsilon_{b\infty})/(\epsilon_{a\infty}+2\epsilon_{b\infty})$. A strong electrostatic contribution is expected in the dispersion for vibron frequencies close to ω_F. In Fig. 2 we depict the electrostatic potential $\Phi_{n_p,1}(r)$ as a function of r for QD radii $R=11.5$ Å, 16.2 Å, and 21 Å. At these radii, $\omega_{n_p,1}$ equals ω_F for $n_p=2$, 3, and 4. It can be seen that the electrostatic potential $\Phi_{n_p,1}$ shows an enhancement close to the interface whenever $\omega_{n_p,1}$ coincides with ω_F.

Now, the results obtained with Eqs. (23)–(26) for the HRS spectrum and resonance profile in CdSe QD's are shown. The incoming (outgoing) resonances will be denoted by the combination of the letter I(O) and the exciton quantum number N of the corresponding resonant levels. It is important to remember the selection rules already discussed in Sec. II: The relevant incoming resonances take place at $2\hbar\omega_l=E_{N,L=1,M,-1}$ whereas the outgoing ones appear at $\hbar\omega_s=E_{N,L=0,0,1}$.

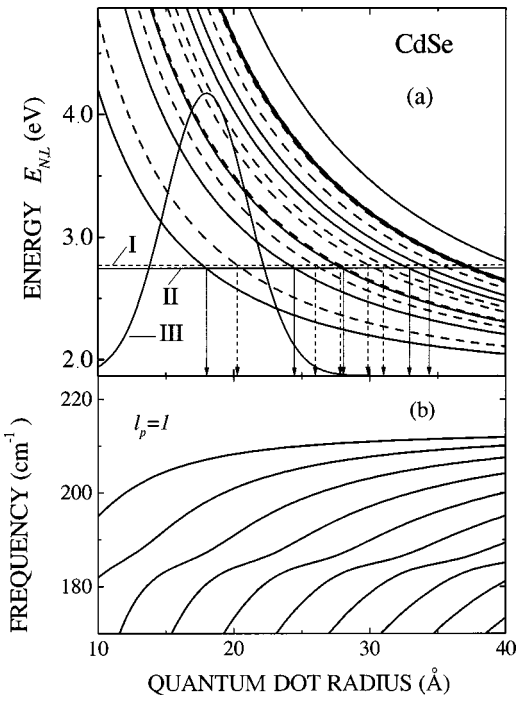

FIG. 1. (a) Energy levels of $N=1,\ldots,7$ and $L=0$ (solid lines) and $L=1$ (dashed lines) excitons in a spherical CdSe nanocrystallite as a function of its radius. Dashed line I indicates the two-photon energy $2\hbar\omega_l=2.771$ eV and solid line II corresponds to the scattered photon energy $\hbar\omega_s=2\hbar\omega_l-\hbar\omega_{1,1}=2.745$ eV. The solid (dashed) arrows indicate the radii of the corresponding outgoing (incoming) resonances. Line III represents a Gaussian distribution over QD radii centered at $\bar{R}=18$ Å and with FWHM equal to 40% (see text). (b) Frequency of the $l_p=1$ optical vibrons of a CdSe nanocrystallite as a function of its radius.

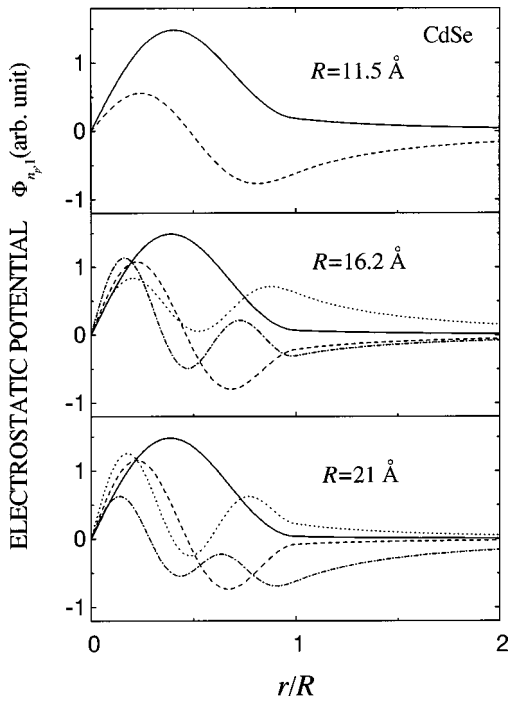

FIG. 2. Plot of the electrostatic potentials associated to the first optical vibrons for different crystallite radii. Solid line, $n_p=1$; dashed line, $n_p=2$; dotted line, $n_p=3$; dot-dashed line, $n_p=4$. The equation $\omega_{n_p,1}(R)=\omega_F$ with $n_p=2$, 3, and 4 is fulfilled for $R=11.5$ Å, $R=16.2$ Å, and $R=21$ Å, respectively. We see that the electrostatic potential $\Phi_{n_p,1}$ increases at the interface whenever $\omega_{n_p,1}$ coincides with the Fröhlich frequency ω_F.

In the next discussion we first analyze the hyper-Raman process for the case in which all nanocrystallites in the sample have the same radius R. Typical HRS spectra are shown in Fig. 3, for different QD radii. The incident photon energy is such that $\hbar\omega_s=2\hbar\omega_l-\hbar\omega_{1,1}$ is in resonance with the $N=1,L=0$ excitonic level. We have included in the calculation the lowest 11 QD excitonic levels ($N=1$ to 11, for each value $L=0,1$). A lifetime broadening $\Gamma_\mu=5$ meV was assumed for all excitonic transitions. The spectra are broadened to have a full width at half maximum (FWHM) $2\Gamma_{n_p}=4$ cm^{-1}. It is systematically found that the main peak of the spectrum corresponds to the creation of the $l_p=1,n_p=1$ vibron, with a small contribution coming from the $n_p=2$, 3, and 4 vibrons. This is related to the fact that the matrix element $\mathcal{H}^{(e,h)}_{\mu_2\to\mu_3}$ drops off rapidly as n_p increases. It must be noted that in the spectra 3(a) and 3(b) the $n_p=3$ peak is stronger than the $n_p=2,4$ ones, while the largest contribution in spectrum 3(c) (aside from the main line) is due to the $n_p=4$ peak. This difference can be explained in terms of the electrostatic effects discussed above: If one looks back to the vibron frequencies as a function of the QD radius in Fig. 1(b), it can be realized that for $R=16$ Å and 18 Å the vibron frequency $\omega_{3,1}$ is around the Fröhlich frequency ω_F, and thus the exciton-vibron interaction is dominant for these modes in the corresponding spectra 3(a) and 3(b). For $R=21$ Å, on the other hand, $\omega_{4,1}$ is approximately equal to

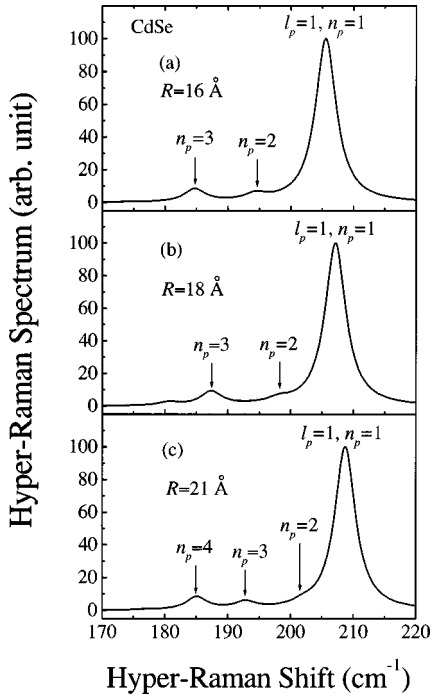

FIG. 3. Hyper-Raman spectra of CdSe nanocrystallites embedded in glass for different radii and two-photon energies: (a) $R=16$ Å and $2\hbar\omega_l=2.975$ eV. (b) $R=18$ Å and $2\hbar\omega_l=2.771$ eV. (c) $R=21$ Å and $2\hbar\omega_l=2.555$ eV.

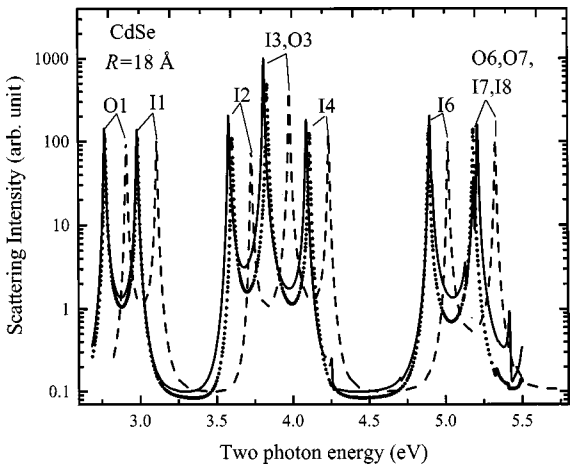

FIG. 4. Hyper-Raman intensity calculated for CdSe nanocrystallites with radius $R=18$ Å. The resonances are denoted by the labels I*N* or O*N*, where I(O) means incoming (outgoing) resonance with the exciton level *N*. Three approaches have been used: Solid line: full matrix diagonalization including exciton effects. Dotted line: first-order perturbation theory for the energy. Dashed line: free electron-hole model.

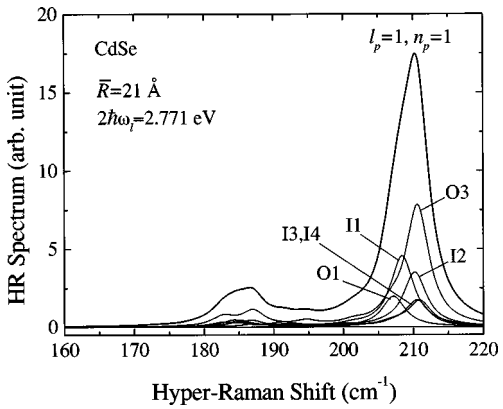

FIG. 5. Hyper-Raman spectrum for $2\hbar\omega_l=2.771$ eV of an ensemble of CdSe QD's with mean radius 21 Å and a 40% size dispersion. The contributions of the QD's with different resonance radii are also shown.

ω_F and, therefore, its potential gives an enhanced contribution to the exciton-vibron interaction (see also Fig. 2), which is reflected in the spectrum 3(c).

The HR resonance profile (scattering efficiency vs $2\hbar\omega_l$) for the $n_p=1,l_p=1$ vibron peak is displayed as a solid line in Fig. 4 for QD radius $R=18$ Å. An important feature of Fig. 4 is that the O1 ($L=0$) resonance takes place at lower energy than the I1 ($L=1$) resonance, which is a natural consequence from the spacing between excitonic levels being much larger than the vibron frequencies. It is worth pointing out that the opposite situation is usually encountered in bulk semiconductors.[23] We have also calculated the HRS intensity taking the Coulomb interaction equal to zero, recovering the free electron-hole model[12] (dashed line), and treating the Coulomb interaction just in first-order perturbation theory (dotted line). It is apparent the exciton redshift when the electron-hole interaction is included. Also, when comparing the absolute values of the scattering intensities for the different approaches we see that the full calculation is extremely well approximated by the perturbative approach and gives only slightly larger values than the free electron-hole model (mainly due to the enhanced oscillator strengths of $L=0$ excitons). Pertaining to the HR cross section the free electron-hole model presents identical line shape to those displayed in Fig. 3, whenever $2\hbar\omega_l$ is rescaled to set the equivalent resonance conditions. Thus, we conclude that the excitonic effects on the HR resonance profile (and also on the HR spectrum) of quantum dots in the strong confinement regime stand mostly to renormalize the resonance energies.

Let us finally discuss the effects of the size dispersion of the crystallites on the HRS spectrum. We have considered an ensemble of QD's described by a Gaussian distribution function $F(R)$ centered at the mean radius $\bar{R}$ and with FWHM equal to 40%. For a given incoming photon energy $\hbar\omega_l$, the conditions $2\hbar\omega_l=E_{\mu_2}$ and $\hbar\omega_s=E_{\mu_3}$ determine a set of resonance radii $\{R_r\}$ and their corresponding resonant exciton levels $\{E_r\}$ with lifetime broadening $\{\Gamma_r\}$. These are marked by arrows in Fig. 1(a), at $2\hbar\omega_l=2.771$ eV. As R departs from R_r, the resonance condition ceases to hold rapidly. The range δR_r around the resonance radius R_r, which contributes to the integral in Eq. (26), is typically of the order of some tens of angstroms. In such a small interval, the matrix elements and the vibron frequencies in Eq. (24) can be considered as constants. On these grounds we have employed the following approximation:

$$\int \frac{d^2\sigma(R)}{d\Omega_s d\omega_s}F(R)dR \rightarrow \sum_r \frac{d^2\sigma(R_r)}{d\Omega_s d\omega_s}F(R_r)\delta R_r . \quad (27)$$

An estimation for δR_r can be obtained from $\delta R_r = \pi\Gamma_r/(dE_r/dR|_{R_r})$. Note that as the HR spectrum evaluated at the resonance radius R_r is proportional to Γ_r^{-2} and δR_r is proportional to Γ_r, the contribution of the R_r-resonant QD's to the average HR spectrum is proportional to $1/\Gamma_r$.

In Fig. 5 we show the averaged HR spectrum of the ensemble of CdSe spherical nanocrystallites with a mean radius of 21 Å, obtained when $2\hbar\omega_l=2.771$ eV. This two-photon energy determines a set of incoming and outgoing resonances with different exciton levels for QD's with different radii R_r, which are listed in Table II (for the emission of the $n_p=1,l_p=1$ vibron). The contributions of the various R_r are also shown in Fig. 5. The resonances due to other exciton levels either are too weak or are attenuated by the size distribution function. Two important features of the HR spectrum deserve special attention. The first one is the main peak at about 208 cm^{-1}, which is originated by the emission of the $n_p=1,l_p=1$ vibrons in QD's with different resonance radii. The most important contribution is that of the outgoing resonance O3, which takes place for $R=28.0$ Å. This reso-

TABLE II. List of resonance radii and corresponding resonant exciton levels (see text and Fig. 5). The incoming (outgoing) resonances are labeled by I*N* (O*N*).

R (Å)	18.0	20.3	26.0	27.8	28.0	30.0
(N,L)	(1,0)	(1,1)	(2,1)	(3,1)	(3,0)	(4,1)
-	O1	I1	I2	I3	O3	I4

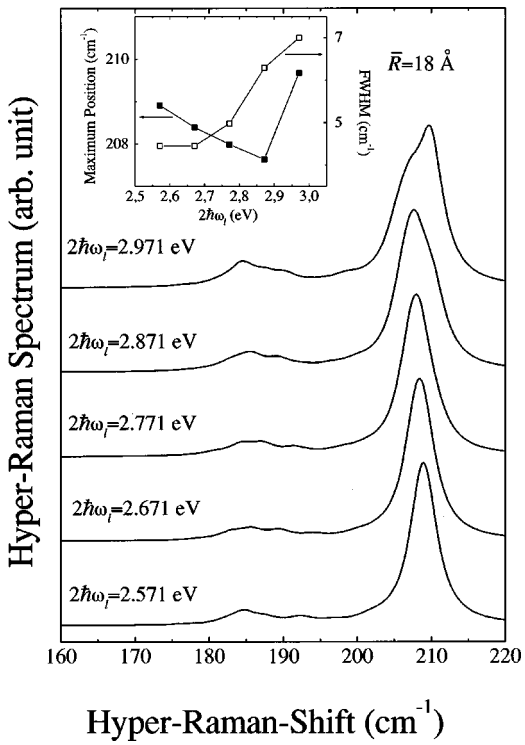

FIG. 6. Hyper-Raman spectra for an ensemble of QD's with a mean radius of 18 Å and a 40% size dispersion for different values of the laser energy. The inset illustrates the dependence of the maximum position and FWHM on the two-photon energy $2\hbar\omega_l$. The lines are a guide to the eyes.

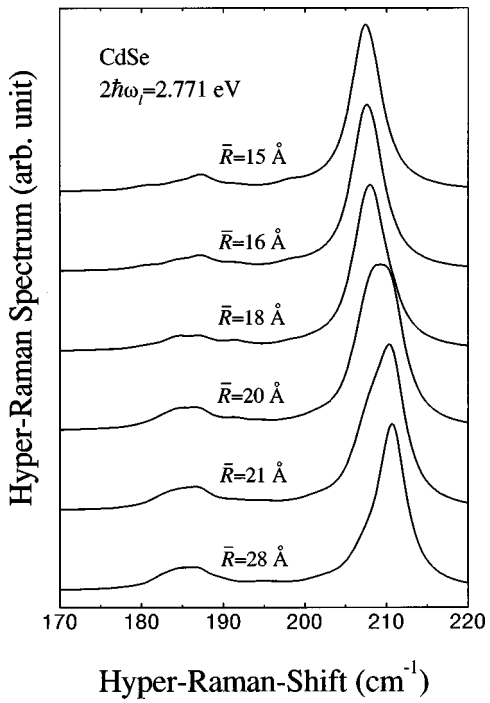

FIG. 7. Dependence of the HR line shape with the mean radius $\bar{R}$ at $2\hbar\omega_l = 2.771$ eV. The size dispersion is 40% of the mean radius in all the spectra.

nance appears so strongly because a double resonance condition connecting the levels $N=3, L=0$, and $N=3$; $L=1$ is almost fulfilled [see Fig. 1(a)]. In addition, the resonance $I3$, associated to dots of radius $R=27.8$ Å, is very close in energy to O3. The second important feature is the broad structure between 180 and 190 cm^{-1}. This structure is caused by the emission of interfacelike vibrons from all resonant QD's. Its irregular shape is a direct consequence of the vibron frequency dispersion as a function of QD radius.

Figure 6 shows the variation of the HR line shape with small variations of the incoming photon energy for an ensemble of QD's with a mean radius of 18 Å. When $2\hbar\omega_l = 2.771$ meV increases (decreases) by 100 meV, the radii of resonance get smaller (larger) by about 1 Å [see Fig. 1(a)]. Hence, the principal peak of the spectrum is shifted to low (high) frequencies, as can be seen in the four lower curves of the figure. Nevertheless, an opposite effect appears in the upper spectrum (change from $2\hbar\omega_l = 2.771$ eV to $2\hbar\omega_l = 2.971$ eV). In this special situation the higher-resonance radii get closer to the mean radius $\bar{R}=18$ Å and become dominant in the spectrum. This effect is equivalent to an increase of the mean radius. It is important to note that the FWHM of the spectrum gradually increases as a result of the competition between the large contributions of the resonance radii.

Finally, the dependence of the HR line shape on the mean radius for $2\hbar\omega_l = 2.771$ eV is shown in Fig. 7. The main features can be explained with similar arguments as in the previous figures. For $\bar{R}=15$ and 16 Å the line shapes are practically identical due to the resonance O1 in the dots of radius $R=18$ Å. For $\bar{R}=18$ Å the maximum is slightly shifted to high frequencies reflecting the influence of other resonances associated with larger radii. For $\bar{R}=20$ Å the main peak is not Lorentzian, showing the contribution of several equally strong resonances. And for $\bar{R}\geqslant 21$ Å the resonance O3 becomes dominant.

The above-presented model might also be applicable to CdS QD's. Nevertheless, the available data reported for this type of QD's[19] are not complete enough to stress the HRS showing the vibron confinement effects. In particular, the experiments of Ref. 19 were realized at room temperature displaying the HR intensity in a wide spectral range with low spectral resolution (~ 25 cm^{-1}). Under these conditions the exciton and vibron confinement effects are not so well observed. We could have performed the calculation anyway and discussed the same effects on fine structure. However, the obtained results for this case would not be so reliable due to uncertainties in the CdS parameters, e.g., hole effective masses and phonon dispersion. Moreover, the interpretation given to the HRS data in Ref. 19 is sufficient and not too much can be argued.

V. CONCLUSIONS

We have performed a theoretical study of the normalized hyper-Raman scattering efficiency in spherical semiconductor quantum dots, considering confined Wannier-Mott excitons as the intermediate states. The exciton-lattice interaction is assumed to occur via Fröhlich-type coupling. It has been shown that hyper-Raman spectroscopy can be used to probe the $l_p=1$ vibrational modes. In addition, each particular mode ($m_p=0,\pm 1$) can be selected by properly choosing the polarization of the incident light. With linearly polarized in-

cident light, only $m_p=0$ vibrons contribute to the scattering whereas by employing circularly polarized light the $m_p=\pm 1$ modes are active. The details of the calculations of the polar optical vibrational modes in CdSe QD's have been discussed and the eigenfrequencies and electrostatic potentials of the $l_p=1$ modes have been presented as a function of the nanocrystallite radius. It has been demonstrated that when their frequencies are close to the Fröhlich frequency, they undergo an increase in their electrostatic surface character.

The calculations of the hyper-Raman spectra show that the most prominent peak is due to the emission of $n_p=1, l_p=1$ vibrons. The other contributions are due to the interfacelike $l_p=1$ vibrons. The presence of surface electronic excitations could increase their role in hyper-Raman scattering.

The effect of the electron-hole Coulomb interaction has been found to be of limited importance for the hyper-Raman scattering in the strong confinement limit relevant to the QD's analyzed here. The absolute values of the HRS intensity are slightly enhanced by the Coulomb interaction as compared to the free electron-hole model values. The main excitonic effect seems to be the renormalization of the resonance energies.

The size dispersion of the nanocrystallites is shown to give rise to a complex behavior of the main peak position in the HR spectrum as a function of the laser energy and the details of the distribution over radii. An additional effect is the distribution of the signal due to interfacelike vibrons over a broad band of frequencies from 180 to 190 cm^{-1}.

ACKNOWLEDGMENTS

One of us (E.M.-P.) acknowledges J. L. Peña for his hospitality at CINVESTAV-IPN (Merida, Mexico), where part of this work was performed. We are grateful to C. Rodriguez-Castellanos for a critical reading of the manuscript.

APPENDIX: REDUCTION OF THE MATRIX ELEMENTS

In this appendix we show in detail how to calculate matrix elements of the form

$$\langle n_e', n_h', l_e', l_h', L', M' | T_{kq} | n_e, n_h, l_e, l_h, L, M \rangle, \quad \text{(A1)}$$

where T_{kq} is the qth component of a kth-order spherical tensor (single-particle) operator T_k, $|n_e, n_h, l_e, l_h, L, M\rangle$ represent an electron-hole pair state, and (L, M) are the corresponding total angular momentum quantum numbers.

First of all, we factorize the dependence on M', M, and q by applying the Wigner-Eckart theorem:

$$\begin{aligned}\langle n_e', n_h', l_e', l_h', L', M' | T_{kq} | n_e, n_h, l_e, l_h, L, M \rangle &= (-1)^{L'-M'} \begin{pmatrix} L' & k & L \\ -M' & q & M \end{pmatrix} \sqrt{2L'+1} \\ &\times \langle n_e', n_h', l_e', l_h', L' \| T_k \| n_e, n_h, l_e, l_h, L \rangle. \end{aligned} \quad \text{(A2)}$$

The factor $\langle \ldots, L' \| T_k \| \ldots, L \rangle$ does not depend on q and is called the *reduced matrix element*. It can be further simplified by taking into account that T_{kq} is a single-particle operator. Let us suppose, without loss of generality, that this operator only acts on the electron coordinates. Then the following reduction formula can be applied:[34]

$$\begin{aligned}\langle n_e', n_h', l_e', l_h', L' \| T_k^{(e)} \| n_e, n_h, l_e, l_h, L \rangle &= \delta_{n_h', n_h} \delta_{l_h' l_h} (-1)^{k+l_h+L+l_e'} \begin{Bmatrix} L' & L & k \\ l_e & l_e' & l_h \end{Bmatrix} \\ &\times \sqrt{(2L+1)(2l_e'+1)} \langle n_e', l_e' \| T_k^{(e)} \| n_e, l_e \rangle. \end{aligned} \quad \text{(A3)}$$

Finally, by inserting Eq. (A3) into Eq. (A2) we achieve the complete simplification of the matrix element (A1).

Let us illustrate this procedure taking as example the matrix element of the operator $\vec{e} \cdot \vec{r}_e$. As a previous step we must realize that the operator $\vec{e} \cdot \vec{r}_e$ can be expressed in terms of spherical irreducible tensors,

$$\vec{e} \cdot \vec{r}_e = \sum_{q=-1}^{1} a_q T_{1q}^{(e)}, \quad T_{1q}^{(e)} = \sqrt{\frac{4\pi}{3}} r_e Y_{1,q}(\Omega_e), \quad \text{(A4)}$$

with the definitions

$$a_0 = e_z, \quad a_{\pm 1} = \frac{i e_y \mp e_x}{\sqrt{2}}. \quad \text{(A5)}$$

Now, by applying Eqs. (A2) and (A3) we obtain

$$\begin{aligned}\langle n_e', n_h', l_e', l_h', L_2, M_2 | \vec{e} \cdot \vec{r}_e | n_e, n_h, l_e, l_h, L_1, M_1 \rangle &= \delta_{n_h', n_h} \delta_{l_h', l_h} a_{M_2 - M_1} (-1)^{1+l_h'+L_1+L_2-M_2} \\ &\times \begin{pmatrix} L_2 & 1 & L_1 \\ -M_2 & M_2 - M_1 & M_1 \end{pmatrix} \begin{Bmatrix} L_2 & L_1 & 1 \\ l_e & l_e' & l_h \end{Bmatrix} \\ &\times \begin{pmatrix} l_e' & 1 & l_e \\ 0 & 0 & 0 \end{pmatrix} \\ &\times \sqrt{(2L_2+1)(2L_1+1)(2l_e'+1)(2l_e+1)} \\ &\times \left(\int R_{n_e', l_e'}(r) R_{n_e, l_e}(r) r^3 dr \right). \end{aligned} \quad \text{(A6)}$$

Proceeding in a similar way it can be shown that an expression analogous to Eq. (A6) (with subscripts e and h exchanged everywhere) holds for the matrix element of the hole operator $\vec{e} \cdot \vec{r}_h$. To obtain the last expression we have used the following reduced matrix elements:

$$\begin{aligned}\langle n', l' \| T_1 \| n, l \rangle &= \sqrt{\frac{4\pi}{3}} \left(\int R_{n', l'}(r) R_{n, l}(r) r^3 dr \right) \\ &\times \langle l' \| Y_1 \| l \rangle, \end{aligned} \quad \text{(A7)}$$

$$\langle l' \| Y_k \| l \rangle = (-1)^{l'} \sqrt{\frac{(2l+1)(2k+1)}{4\pi}} \begin{pmatrix} l' & k & l \\ 0 & 0 & 0 \end{pmatrix}. \quad \text{(A8)}$$

Moreover, if we particularize Eq. (A6) to the case $L_1=M_1=0$ ($l_e=l_h$) and evaluate the $3j$ and $6j$ symbols we get the result shown in Eq. (13).

Applying the same method the following expression is obtained for the matrix elements of the electron-lattice interaction:

$$\langle n_e'' n_h'' l_e'' l_h'' L_3 M_3 | e\hat{\varphi}_F(\vec{r}_e) | n_e' n_h' l_e' l_h' L_2 M_2 \rangle$$

$$= \delta_{n_h',n_h''}\delta_{l_h',l_h''}(-1)^{L_2+L_3+l_h'-M_2}\sum_{n_p,l_p,m_p}(-1)^{l_p}\frac{C_F}{\sqrt{R}} \times\sqrt{(2L_2+1)(2L_3+1)} \times\sqrt{(2l_e'+1)(2l_e''+1)(2l_p+1)/4\pi} \times\begin{pmatrix} L_2 & l_p & L_3 \\ -M_2 & m_p & M_3\end{pmatrix}\begin{pmatrix} l_e' & l_p & l_e'' \\ 0 & 0 & 0\end{pmatrix} \times\begin{Bmatrix} L_2 & L_3 & l_p \\ l_e'' & l_e' & l_h'\end{Bmatrix}\Phi^{n_p,l_p}_{n_e'',l_e''\to n_e',l_e'}. \quad \text{(A9)}$$

In this expression it is implicit that only the creation part of $\hat{\varphi}_F$ is acting on the ket. Replacing $L_2=1, L_3=M_3=0$, the Eq. (A8) is reduced to Eq. (19) and $\Phi^{n_p,l_p}_{n_e'',l_e''\to n_e',l_e'}$ is defined in Eq. (20).

[1] C. W. Beenaker and H. van Houten, in *Solid State Physics: Semiconductor Heterostructures and Nanostructures*, edited by H. Ehrenreich and D. Thurnbull (Academic Press, San Diego, CA, 1991), Vol. 44.

[2] U. Woggon and S. V. Gaponenko, Phys. Status Solidi B **189**, 285 (1995).

[3] M. Cardona, in *Light Scattering in Solids II*, edited by M. Cardona and G. Güntherodt, Topics in Applied Physics Vol. 50 (Springer, Heidelberg, 1982), p. 19.

[4] T. D. Krauss, F. W. Wise, and D. B. Tanner, Phys. Rev. Lett. **76**, 1376 (1996).

[5] P. T. C. Freire, M. A. Araujo Silva, V. C. S. Reynoso, A. R. Vay, and V. Lemos, Phys. Rev. B **55**, 6743 (1997).

[6] G. Scamarcio, M. Lugara, and D. Manno, Phys. Rev. B **45**, 13 792 (1992).

[7] Al. L. Efros, A. I. Ekimov, F. Kozlowsky, V. Petrova-Koch, M. Schmidbaur, and S. Shumilov, Solid State Commun. **78**, 853 (1991).

[8] A. V. Fedorov, A. V. Baranov, and K. Inoue, Phys. Rev. B **56**, 7491 (1997).

[9] M. C. Klein, F. Hache, D. Ricard, and C. Flytzanis, Phys. Rev. B **42**, 11 123 (1990).

[10] C. Trallero-Giner, A. Debernardi, M. Cardona, E. Menéndez-Proupin, and A. I. Ekimov, Phys. Rev. B **57**, 4664 (1998).

[11] C. Trallero-Giner, F. Garcia-Moliner, V. R. Velasco, and M. Cardona, Phys. Rev. B **45**, 11 944 (1992).

[12] M. P. Chamberlain, M. Cardona, and B. K. Ridley, Phys. Rev. B **48**, 14 356 (1993).

[13] C. Trallero-Giner, F. Comas, and F. Garcia-Moliner, Phys. Rev. B **50**, 1755 (1994).

[14] A. J. Shields, M. Cardona, and K. Eberl, Phys. Rev. Lett. **72**, 412 (1994).

[15] E. Roca, C. Trallero-Giner, and M. Cardona, Phys. Rev. B **49**, 13 704 (1994).

[16] M. P. Chamberlain, C. Trallero-Giner, and M. Cardona, Phys. Rev. B **51**, 1680 (1995).

[17] E. Menendez, C. Trallero-Giner, and M. Cardona, Phys. Status Solidi B **199**, 81 (1997); **201**, 551 (1997).

[18] V. N. Denisov, B. N. Mavrin, and V. B. Podobedov, Phys. Rep. **151**, 1 (1987).

[19] A. V. Baranov, K. Inoue, K. Toba, A. Yamanaka, V. I. Petrov, and A. V. Fedorov, Phys. Rev. B **53**, R1721 (1996).

[20] K. Inoue, K. Toba, A. Yamanaka, A. V. Baranov, A. A. Onushchenko, and A. V. Fedorov, Phys. Rev. B **54**, R8321 (1996).

[21] A. V. Fedorov, A. V. Baranov, and K. Inoue, Phys. Rev. B **54**, 8627 (1996).

[22] M. D. Levenson, *Introduction to Nonlinear Laser Spectroscopy* (Academic Press, New York, 1982).

[23] A. Garcia-Cristobal, A. Cantarero, C. Trallero-Giner, and M. Cardona, Phys. Rev. B **58**, 10 443 (1998).

[24] C. Trallero-Giner, A. Cantarero, and M. Cardona, Phys. Rev. B **40**, 4030 (1989).

[25] J. D. Jackson, *Classical Electrodinamics* (Wiley, New York, 1962).

[26] K. C. Rustagi, F. Pradere, and A. Mysyrowicz, Phys. Rev. B **8**, 2721 (1973).

[27] A. Debernardi and M. Cardona (private communication).

[28] R. Fuchs and K. L. Kliewer, Phys. Rev. **140**, A2076 (1965); R. Ruppin and R. Englman, Rep. Prog. Phys. **33**, 149 (1970).

[29] H. Fröhlich, *Theory of Dielectrics* (Oxford University Press, Oxford, 1948).

[30] Landolt-Börnstein, *Numerical Data and Functional Relationships in Science and Technology*, edited by O. Madelung, Group III, Vol. 17 (Springer-Verlag, Berlin, 1982).

[31] R. G. Alonso, E. Suh, A. K. Ramdas, H. Luo, and J. K. Furdyna, Phys. Rev. B **40**, 3720 (1989).

[32] W. L Wolf, S. B. Stanley, and K. A. McCarty, *American Institute of Physics Handbook* (McGraw-Hill, New York, 1963), p. 24.

[33] C. Hermann and C. Weisbuch, Phys. Rev. B **15**, 823 (1977).

[34] D. M. Brink and G. R. Satcher, *Angular Momentum* (Clarendon Press, Oxford, 1968).